

ANALYSIS OF WAVE FORCES ACTING ON COMBINED CAISSONS WITH INNER SLOPE RUBBLE MOUND

Carla Faraci¹, Yong Liu²

This study examines the horizontal wave forces acting on combined caissons with inner slope rubble mound based on the semi-analytical solution of Liu and Faraci (2014). The calculating method of the horizontal wave forces are presented and validated. The effects of several caisson parameters on the wave forces are shown using some numerical examples. Some useful results are presented for engineering designs.

Keywords: Combined caisson; slope rubble mound; wave force; semi-analytical solution

Introduction

A new combined caisson has been recently used in Italy for several harbor enlargements. The combined caisson has a large window on the front wall near the still water level, and it is filled with rubble mound with a slope, as shown in Figure 1. The incident waves can come into the caisson through the front window and the incident wave energy may be partially dissipated by the rubble mound slope. As a result, the reflection coefficient of the structure is reduced, which is of primary engineering interest, but at the same time the space occupied by the caisson is restrained.

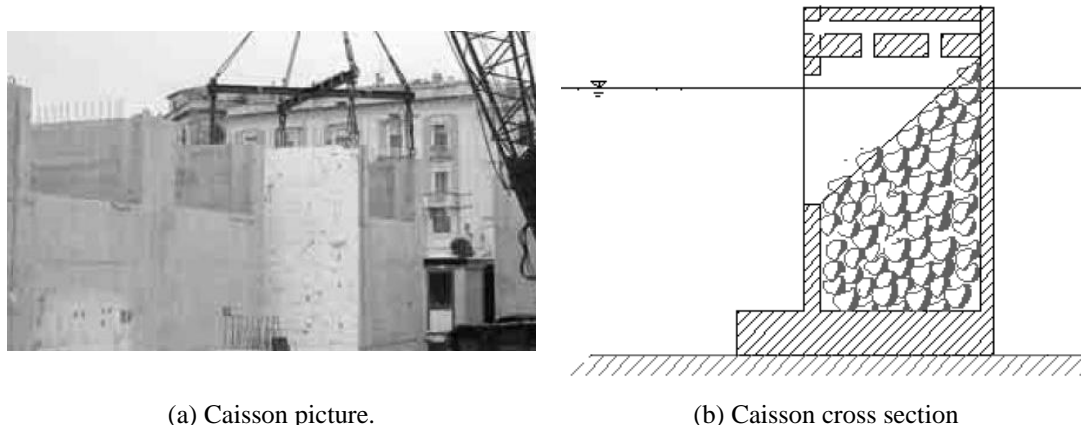


Figure 1. Combined caissons in the Siracusa harbor (Italy).

Wave reflections by combined caissons and similar structures have been studied in the last two decades (e.g., Matteotti, 1991; Theocharis et al., 2011; Altomare and Gironella, 2014; Faraci et al., 2014; Liu and Faraci, 2014). Matteotti (1991) proposed and experimentally examined a quay wall with an inner sloping rubble mound near the free surface. They found that the quay wall may attain low reflection. Theocharis et al. (2011) experimentally studied a quay wall with a wave-absorbing chamber filled with a rock armored slope, which was used in Piraeus Port, Greece. They found that compared to the traditional solid vertical wall, the wave height in front of the wave-absorbing quay wall was reduced by 20 – 30%. Recently, Altomare and Gironella (2014) gave empirical formulas for estimating reflection coefficients of low reflective quay walls with inner slope rubble mounds, and examined the scale effect of inner slope rubble mound. Faraci et al. (2014) and Liu and Faraci (2014) examined the reflection coefficients of combined caissons by means of experimental tests and semi-analytical solution, respectively. Both the studies confirmed the best wave absorbing performance (low reflection coefficient) of suitably designed combined caissons. The minimum reflection coefficient of combined caisson may attain 0.1 – 0.3 (Faraci et al, 2014). All the preceding studies examined the reflection coefficients of combined caissons and similar structures, but the stability of such structures was less carefully examined so far.

¹ Department of Civil and Environmental Engineering, Computer Science, Building and Applied Mathematics (DICIEAMA), University of Messina, C.da di Dio, Messina, 98166, Italy

² Shandong Provincial Key Laboratory of Ocean Engineering, Ocean University of China, Qingdao 266100, China

In this work the wave forces acting on combined caissons are calculated and analyzed based on the semi-analytical solution of Liu and Faraci (2014). The analytical method for calculating the wave forces on combined caissons is presented in the next section. In section 3, the wave forces predicted by the semi-analytical solution are validated using a multi-domain boundary element method (BEM) solution. In section 4, numerical examples for wave forces acting on combined caissons are presented with discussions. Finally, the main conclusions of this study are drawn.

Analytical method for calculating wave forces

Wave action on a combined caisson with an inner slope rubble mound is sketched in Figure 2. The combined caisson is located in the sea with a constant depth d . The caisson chamber width is b and the submerged depth of the front vertical wall is h_1 . The height of front wall is a , and $a = d - h_1$. The width of inner rubble mound at the still wave level is b_{swl} . The slope of inner rubble mound is γ and $\gamma = h_1 / (b - b_{swl})$. The whole structure is subject to linear time-harmonic waves with wave period T , wavelength L and wave height H . A Cartesian coordinate system, with the z -axis along the chamber rear wall and directing upwards from the still water level, and the x -axis pointing out of the fluid domain, is used for descriptions.

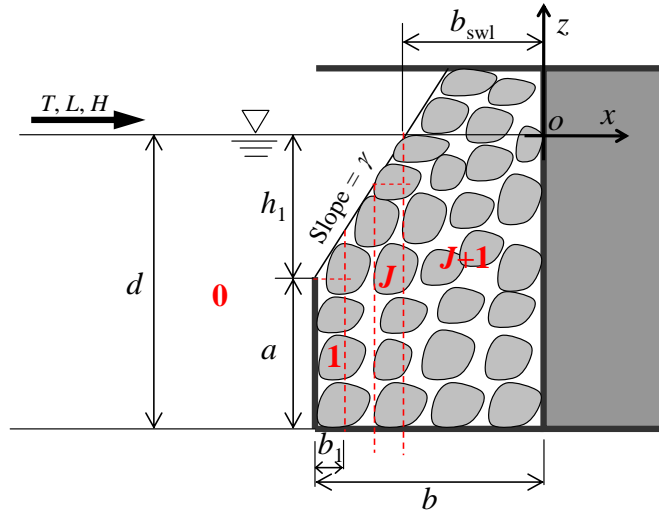


Figure 2. Sketch for wave action on a combined caisson with an inner slope rubble mound.

Liu and Faraci (2014) developed a semi-analytical solution for wave reflection by the combined caisson in Figure 2 using linear potential theory. In the solution of Liu and Faraci (2014), the inner rubble mound was treated as a rigid, homogenous and isotropic porous medium (Sollitt and Cross, 1972), which was represented by the resistance coefficient f , the inertial coefficient s and the porosity ε . The inner slope rubble mound was further treated as a series of horizontal porous steps. Then, the velocity potentials in each step region were determined by matched eigenfunction expansions and the reflection coefficient was estimated. Here we use the velocity potentials obtained by Liu and Faraci (2014) to calculate and analyze the wave forces acting on combined caissons. We need the velocity potentials in the seaside and lee side regions of the front wall (region 0 and region 1... J) and the velocity potential in region $J + 1$ (the surface-piercing rubble mound region). The slope rubble mound is represented by J artificial steps and the first step is located in region 1. The velocity potentials in regions 0, 1 and $J + 1$ are respectively given by (Liu and Faraci, 2014):

$$\phi^{(0)} = \frac{-igH}{2\omega} \left\{ \left[e^{ik_0(x+b)} + R_0 e^{-ik_0(x+b)} \right] Z_0(z) + \sum_{m=1}^{\infty} R_m e^{k_m(x+b)} Z_m(z) \right\}, \quad (1)$$

$$\phi^{(1)} = \frac{-igH}{2\omega} \sum_{m=0}^{\infty} \left[A_m e^{i\lambda_m(x+b)} + C_m e^{-i\lambda_m(x+b-h_1)} \right] Y_m(z), \quad (2)$$

$$\phi^{(J+1)} = \frac{-igH}{2\omega} \sum_{m=0}^{\infty} D_m \frac{\cos \alpha_m x}{\cos \alpha_m b_{swl}} X_m(z), \quad (3)$$

where g is the acceleration of gravity; ω is the angular frequency of incident waves; $Z_m(z)$, $Y_m(z)$ and $X_m(z)$ are vertical eigenfunctions; k_m , λ_m and α_m are eigenvalues; and R_m , A_m , C_m and D_m are unknown expansion coefficients, which must be determined by matching boundary conditions among different regions. The relevant details can be found in Liu and Faraci (2014). The eigenvalues k_m are the positive roots of following dispersion relations:

$$\omega^2 = gk_0 \tanh k_0 d = -gk_m \tan k_m d, \quad m = 1, 2, \dots \quad (4)$$

In fact, k_0 is the incident wave number, $k_0 = 2\pi / L$. The eigenvalues λ_m and α_m satisfy the following complex dispersion relations:

$$\omega^2 - g\lambda_m \tanh \lambda_m d = P_m [\omega^2 \tanh \lambda_m d - g\lambda_m], \quad m = 0, 1, 2, \dots \quad (5)$$

$$(s + if)\omega^2 = g\alpha_m \tanh \alpha_m d, \quad m = 0, 1, 2, \dots \quad (6)$$

where

$$P_m = \frac{[1 - \varepsilon/(s + if)] \tanh \lambda_m a}{1 - \varepsilon/(s + if) \tanh^2 \lambda_m a}, \quad m = 0, 1, 2, \dots \quad (7)$$

The dynamic pressure in the fluid domain can be calculated by (Sollitt and Cross, 1972):

$$p = (s + if)i\rho\omega\phi, \quad (8)$$

where ρ is the fluid density. In region 0, there is no porous medium ($s = 1$ and $f = 0$). Then, Eq. (8) reduces to the usual linear Bernoulli equation. The magnitude of wave force acting on the front wall is calculated by

$$F_f = i\rho\omega \int_{-d}^{-h} [\phi^{(0)}(-b, z) dz - (s + if)\phi^{(1)}(-b, z)] dz \\ = \frac{\rho g H}{2} \left\{ (1 + R_0)\Lambda_0 + \sum_{m=1}^{\infty} R_m \Lambda_m - (s + if) \sum_{m=0}^{\infty} (A_m + C_m e^{i\lambda_m h}) \Gamma_m \right\}, \quad (9)$$

where

$$\Lambda_0 = \sinh k_0 a / (k_0 \cosh k_0 d), \quad (10)$$

$$\Lambda_m = \sin k_m a / (k_m \cos k_m d), \quad m = 1, 2, \dots, \quad (11)$$

$$\Gamma_m = \frac{(1 - P_m \tanh \lambda_m a) \sinh \lambda_m a}{\lambda_m (s + if) (\cosh \lambda_m h - P_m \sinh \lambda_m h)}, \quad m = 0, 1, 2, \dots, \quad (12)$$

The magnitude of wave force acting on the chamber rear wall is calculated by

$$F_r = (s + if)i\rho\omega \int_{-d}^0 \phi^{(J+1)}(0, z) dz = \frac{\rho g H}{2} \sum_{m=0}^{\infty} \frac{D_m \tanh \alpha_m d}{\alpha_m \cos \alpha_m b_{swl}}. \quad (13)$$

Then, the magnitude of the total horizontal wave force acting on combined caisson is given by:

$$F_t = F_f + F_r. \quad (14)$$

The dimensionless wave forces are defined as

$$C_{Fi} = \left| \frac{F_i}{\rho g H d} \right|, \quad (15)$$

$$C_{Ff} = \left| \frac{F_f}{\rho g H d} \right|, \quad (16)$$

$$C_{Fr} = \left| \frac{F_r}{\rho g H d} \right|. \quad (17)$$

Following Liu and Faraci (2014), the resistance coefficient f for the inner slope rubble mound is estimated by:

$$f = (Dk_0)^{-0.57}, \quad (18)$$

where D is the characteristic stone diameter. The resistance coefficient estimated by Eq. (18) is larger than that by the formula in Pérez Romero et al. (2009) for a vertical porous rubble mound. This is due to the additional energy dissipation by the surface turbulence on the slope rubble mound. In the following calculations, a reasonable value of $D/d = 1/9$ is adopted for estimating the resistance coefficient f . The inertial coefficient s is simply treated as unity as usual. The porosity of the inner rubble mound is fixed at $\varepsilon = 0.42$. In addition, the series solutions of velocity potentials in Eqs. (1) – (3) are truncated after 30 terms, and the inner slope is divided into 30 steps. These are the same as that adopted in Liu and Faraci (2014), which can ensure the convergence of the present predictions for wave forces.

Validation

We independently develop a numerical solution for wave action on combined caissons using a multi-domain boundary element method (BEM). The multi-domain BEM solution is a cumbersome numerical solution. We adopt the fundamental solution of Laplace equation given by

$$G(x, z; \xi, \eta) = \ln \sqrt{(x - \xi)^2 + (z - \eta)^2} / (2\pi) \quad (19)$$

where (ξ, η) and (x, y) denote respectively the source point and the field point on the fluid boundaries. All the boundary curves are divided into many smooth elements, and the velocity potential and its derivative on each element are both assumed to be constant. Details on the multi-domain BEM solution can be found in Liu et al. (2012). The slope boundary of the inner rubble mound is also directly divided into many constant elements. Thus, no step approximation is adopted in the multi-domain BEM solution.

The wave forces calculated by the semi-analytical solution and the multi-domain BEM solution are compared, and a typical compared result is shown in Figure 3. It can be seen from Figure 3 that the agreement between the two solutions is very good. This means that the semi-analytical solution based on the step approximation can correctly estimate the wave forces acting on combined caissons. Figure 3 also shows that the wave force acting on the rear wall C_{Fr} may be large. However, due to the phase difference between the wave forces acting on the front and rear walls, C_{Ff} and C_{Fr} , the total wave force C_{Fi} acting on combined caisson is much smaller than C_{Fr} .

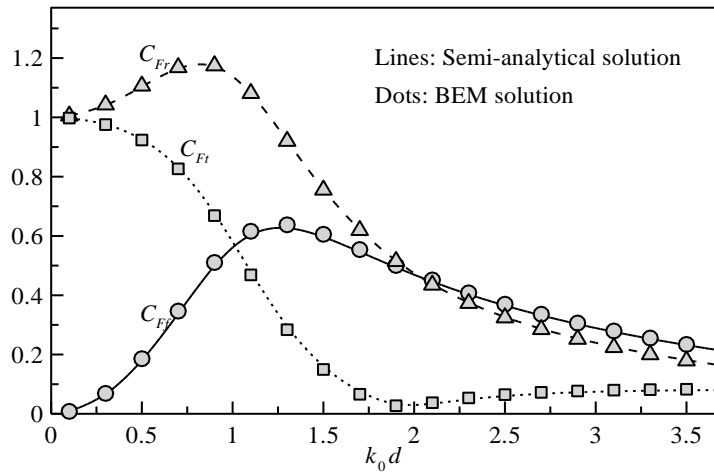


Figure 3 Comparison between the semi-analytical solution and the multi-domain BEM solution at: $h_1 = 0.2d$, $b = 0.5d$ and $\gamma = 1:1.5$.

Numerical examples

According to Liu and Faraci (2014), the relevant parameters mostly affecting the reflection coefficient of combined caisson are the slope γ , the front wall submerged depth h_1 and the surface-piercing rubble mound width b_{swl} (or caisson chamber width b). Here, the effects of these parameters on wave forces acting on combined caissons are examined using numerical examples.

The effect of the rubble mound slope γ on the dimensionless total wave force C_{Ft} is shown in Figure 4. If the combined caisson has no window on the front wall, the present caisson will reduce to the traditional non-perforated caisson (i.e. a vertical solid wall). Based on linear potential theory, the dimensionless standing wave force acting on a vertical solid wall is calculated by

$$C_{Ft} = \tanh(k_0d)/(k_0d). \tag{20}$$

For comparisons, the wave force on a solid vertical wall calculated by Eq. (20) is also added in Figure 4. It can be seen from Figure 4 that the total wave force acting on the combined caisson is generally much smaller than that acting on the traditional caisson with solid front wall. This is very beneficial to enhance the stability of combined caisson. In addition, the total wave force decreases remarkably with the decreasing rubble mound slope, when k_0d is about 0.75 – 1.75. Liu and Faraci (2014) have shown that the combined caisson with gentler slope may generally have smaller reflection coefficient. Thus, a gentler slope is recommended for combined caisson to attain better wave-absorbing performance and smaller wave forces.

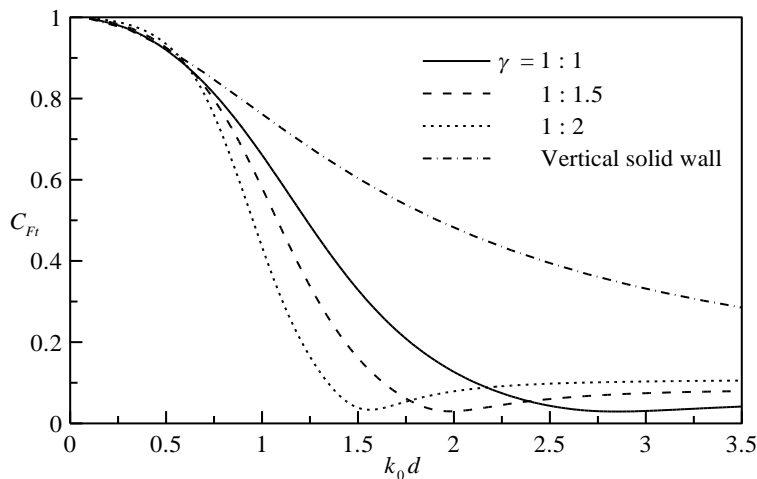


Figure 4 Effect of the rubble mound slope γ on C_{Ft} at: $h_1 = 0.2d$ and $b_{swl} = 0.2d$.

Figure 5 represents the effect of the front wall submerged depth h_1 on the dimensionless total wave force C_{Ft} . It is evident from Figure 5 that the variation of total wave force with the decreasing submerged depth of front wall is not significant. We further examine wave forces acting on the front and rear walls (C_{Ff} and C_{Fr}) and find that the values of C_{Ff} and C_{Fr} generally decrease both with the increasing value of h_1 . But the wave forces acting on the front and rear walls have a rather complicated phase difference. As a result, the resultant force C_{Ft} is insensitive to the front wall submerged depth h_1 , as shown in Figure 5.

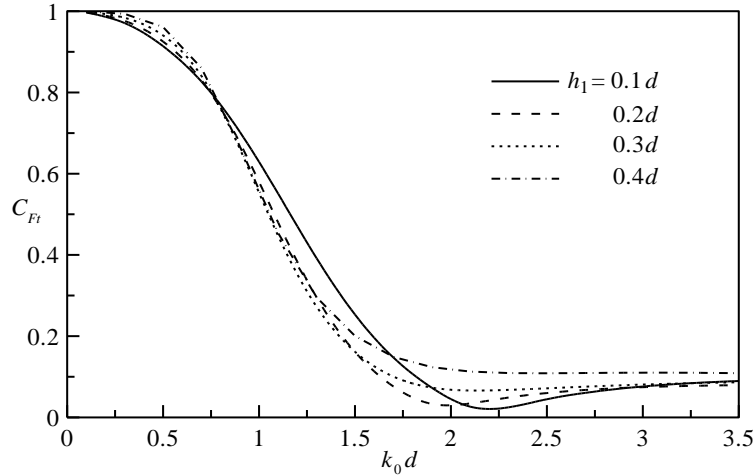


Figure 5 Effect of the front wall submerged depth h_1 on C_{Ft} at: $\gamma = 1:1.5$ and $b_{swl} = 0.2d$.

The effects of the relative chamber width b/L on the wave forces C_{Ff} , C_{Fr} and C_{Ft} are shown in Figure 6. In this figure, the values of $k_0 d$, γ and h_1 are all fixed, only the surface-piercing rubble mound width b_{swl} is increased. For reference, the calculated reflection coefficient C_R of Liu and Faraci (2014) is also added in Figure 6. When the relative chamber width increases, the reflection coefficient attains saturation regime at about $b/L = 0.2$. The saturation regime of reflection coefficient for porous breakwater has been well discussed in Pérez Romero et al. (2009). It can be seen from Figure 6 that with the increasing relative chamber width, the variations of wave forces are somewhat similar to that of the reflection coefficient. With the increasing value of b/L , the wave force on the rear wall C_{Fr} decreases to zero. This should be natural in physics. When the incident waves propagate in the rubble mound, the wave energy is dissipated continuously. If the rubble mound width is large enough, the wave energy will be totally dissipated and no waves can reach the rear wall. Then, the wave force acting on the rear wall is zero. When the relative chamber width increases, the wave force on the front wall C_{Ff} decreases to a constant, while the total wave force C_{Ft} first decreases, attains its minimum and then increase to the same constant of C_{Ff} . For the case in Figure 6, the optimum value of $b/L = 0.15 - 0.2$ is recommend for the combined caisson to attain lower values of both total wave force and reflection coefficient.

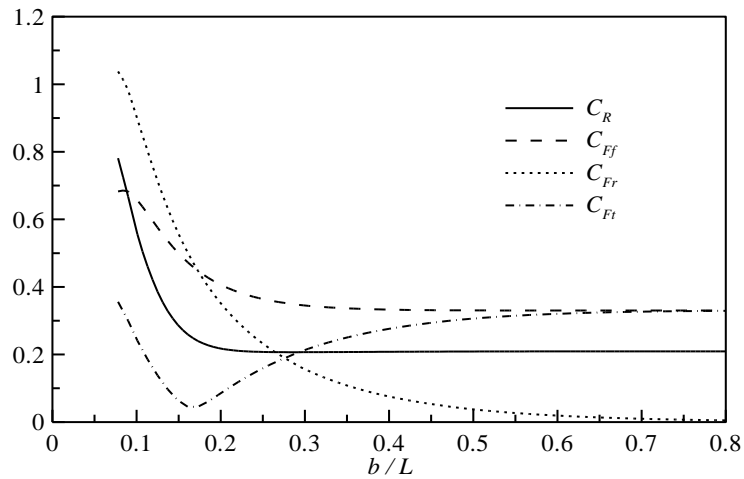


Figure 6 Effects of the relative chamber width b / L on C_{Ff} , C_{Fr} , C_{Ft} and C_R at: $k_0d = 1.5$, $\gamma = 1:1.5$ and $h_1 = 0.2d$.

Finally, we provide Figures 7 and 8 to analyze the effects of γ , h_1 and b_{swl} on C_{Ft} when the chamber width b is fixed, which may be required in practice. In Figure 7, the surface-piercing rubble mound width b_{swl} is fixed, and the slope γ and the front wall submerged depth h_1 are changed. We have found from preceding Figures 4 and 5 that compared to the front wall submerged depth h_1 , the slope γ has much more significant effect on the total wave force C_{Ft} . Thus, the variation of wave forces with the decreasing rubble mound slope γ in Figure 7 is similar to that in Figure 4. In Figure 8, the front wall submerged depth h_1 is fixed, and the slope γ and the surface-piercing rubble mound width b_{swl} are simultaneously reduced. According to Figures 4 and 6, the values of γ and b_{swl} both have significant effects on the total wave force C_{Ft} . However, their effects may be balanced in Figure 8.

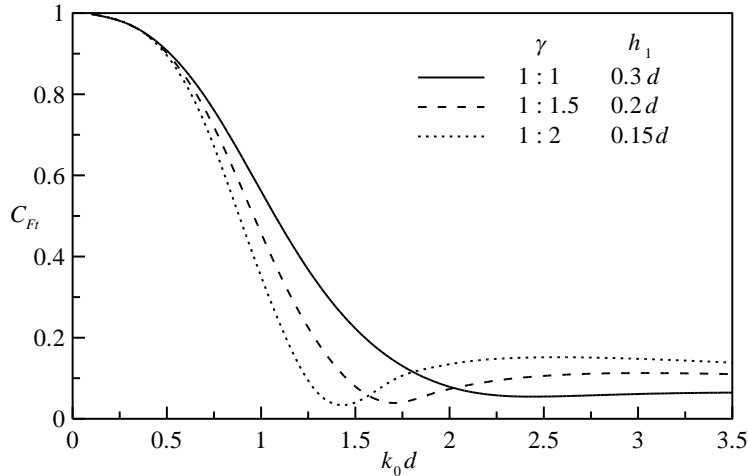


Figure 7 Combined effects of γ and h_1 on C_{Ft} at: $b = 0.6d$ and $b_{swl} = 0.3d$.

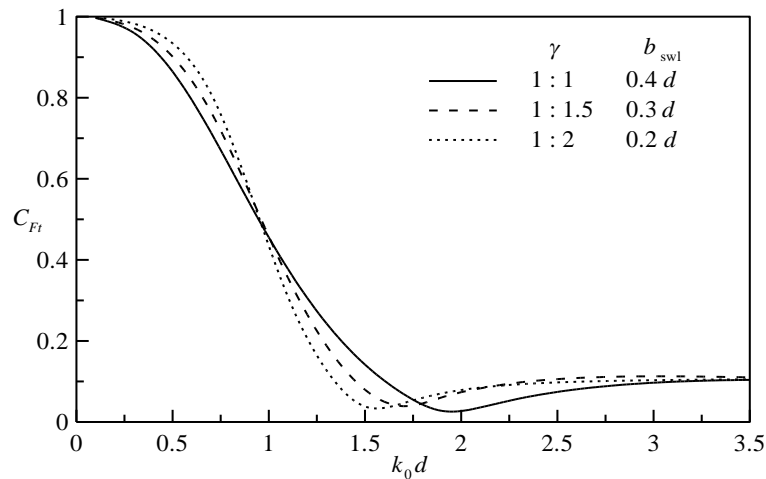


Figure 8 Combined effects of γ and b_{sw1} on C_{Ft} at: $b = 0.6d$ and $h_1 = 0.2d$.

Concluding Remarks

Using the semi-analytical solution of Liu and Faraci (2014) for wave reflection by combined caissons with inner slope rubble mound, we have provided an analytical method for calculating horizontal wave forces acting on combined caissons. The calculated results of wave forces have been validated using a multi-domain BEM solution. Numerical examples have also been presented to examine the effects of several relevant parameters on wave forces. We have found that the total horizontal wave force acting on the combined caisson is much smaller than that on the traditional non-perforated caisson. The total wave force is insensitive to the front wall submerged depth. But, a smaller rubble mound slope or a larger surface-piercing rubble mound width may generally lead to lower total horizontal wave force.

Based on the present analysis results, experimental tests may be carried out to further examine wave forces acting on combined caissons in the future. Besides horizontal wave forces, the vertical wave forces acting on combined caisson should be carefully examined. Finally, according to the study of Liu et al. (2008) for Jarlan-type perforated caissons, the maximum total horizontal and vertical wave forces acting on combined caissons might have a large phase difference, which is very beneficial to enhancing the caisson stability.

ACKNOWLEDGMENTS

This work was partly supported by PRIN 2012 project (2012BYTPR5 - Modellazione di processi idromorfodinamici costieri per applicazioni ingegneristiche). The second author was supported by the National Natural Science Foundation of China (Project Nos. 51322903 and 51279224).

REFERENCES

- Altomare, C., Gironella, X., (2014). An experimental study on scale effects in wave reflection of low-reflective quay walls with internal rubble mound for regular and random waves. *Coastal Engineering* 90, 51–63.
- Faraci, C., Scandura, P., Foti, E., (2014). Reflection of sea waves by combined caissons. *Journal of Waterway, Port, Coastal and Ocean Engineering*, DOI: 10.1061/(ASCE)WW.1943-5460.0000275.
- Liu, Y., Faraci, C., (2014). Analysis of wave reflection by combined caissons with internal rubble mound. *Coastal Engineering*, 91, 151–163.
- Liu, Y., Li, H.J., Li, Y.C. (2012). A new analytical solution for wave scattering by a submerged horizontal porous plate with finite thickness. *Ocean Engineering* 42, 83–92.
- Liu, Y., Li, Y.C., Teng, B., Jiang, J.J., Ma, B.L., (2008). Total horizontal and vertical forces of irregular waves on partially perforated caisson breakwaters. *Coastal Engineering* 55(6), 537–552.
- Matteotti, G., (1991). The reflection coefficient of a wave dissipating quay wall. *The Dock and Harbour Authority* 71(825), 285–291.
- Pérez Romero D.M., Ortega Sanchez, M., Monino, A., Losada M.A., (2009). Characteristic friction coefficient and scale effects in oscillatory porous flow. *Coastal Engineering* 56, 937–939.

- Sollitt, C.K., Cross, R.H., (1972). Wave transmission through permeable breakwaters. In: *Proceedings of the 13th Coastal Engineering Conference*, Vancouver, pp. 1827–1846.
- Theocharis, I., Anastasaki E.N., Moutzouris, C.I., Giantsi T., (2011). A new wave absorbing quay-wall for wave height reduction in a harbor basin. *Ocean Engineering* 38, 1967–1978.